J Solid State Electrochem (2012) 16:1049–1054
DOI 10.1007/s10008-011-1485-6

ORIGINAL PAPER

Carbon-supported platinum-decorated nickel nanoparticles for enhanced methanol oxidation in acid media

Xingli Wang · Hui Wang · Rongfang Wang · Qizhao Wang · Ziqiang Lei

Received: 23 March 2011 / Revised: 16 June 2011 / Accepted: 18 June 2011 / Published online: 12 July 2011

Abstract Carbon-supported platinum-decorated nickel nanoparticles (denoted as Pt-Ni/C) with intimate contact of Pt and Ni are prepared by a galvanic displacement reaction between Ni/C nanoparticles and $PtCl_6^{2-}$ in aqueous solution. It demonstrates a higher mass activity and stability to methanol oxidation reaction than conventional Pt/C and PtRu/C catalysts by a rotating disk electrode in acid solution, which could be attributed to the modified electronic structure of the Pt-Ni/C nanoparticles.

Key words Electrocatalysts · Fuel cells · Methanol oxidation · Low platinum · Galvanic displacement reaction

Introduction

The high electrocatalyst cost and poor anode performance are two key handicaps which restrain the commercialization of the direct methanol fuel cells (DMFCs). The fabrication of low-loaded but active Pt catalysts for the anode is essential for the DMFCs development [1]. Therefore, many efforts have focused on the development of techniques and new materials to achieve high catalytic activity and utilization efficiency.

PtNi alloy catalyst has been much investigated and exhibits an enhanced electrocatalytic activity for oxygen reduction reaction with respective to Pt alone [2–7]. Such an activity enhancement was explained by the increased Pt d-band vacancy (electronic factor) and by the favorable Pt–Pt interatomic distance (geometric effect) [3, 4]. The use of PtNi alloy as DMFC cathodes has also been investigated [8–12]. However, these catalysts were alloy powders with high precious metal loading or not supported on carbon.

Surface modifications of the catalysts at an atomic scale are suggested in an effort to improve the utilization efficiency of active materials and to enhance the electrocatalytic activities in processes of methanol oxidation [13]. Recently, Pt-rich shell-coated Ni nanoparticles as catalysts for methanol electro-oxidation in alkaline media have been studied [14]. However, the stability of the nanoparticles has not been reported. Based on these literature findings, we think it meaningful to explore the carbon-supported Pt-decorated Ni catalyst prepared by chemical reduction for methanol oxidation in acid media. We have recently developed a two-step reduction method to prepare carbon supported PdCu-Pt and PdCu-PtRu electrocatalysts, which have demonstrated higher mass activity than the conventional Pt/C and PtRu/C catalysts in DMFCs [15, 16]. In this article, we modified this method to prepare carbon supported platinum-decorated nickel nanoparticles (Pt-Ni/C) as electrocatalyst and tested its methanol oxidation activity and stability in a three-compartment electrochemical cell.

Experimental

Pt-Ni/C catalyst was prepared by a two-step method. In a typical process, a Ni/C catalyst was prepared as follows: nickel (II) chloride hexahydrate ($NiCl_2 \cdot 6H_2O$) (303 mg) and sodium citrate (750 mg) were dissolved in ethylene glycol (EG) and stirred for 0.5 h. Pretreated carbon black

X. Wang · H. Wang · R. Wang (✉) · Q. Wang · Z. Lei (✉)
Key Laboratory of Eco-Environment-Related Polymer Materials, Ministry of Education of China, Key Laboratory of Gansu Polymer Materials, College of Chemistry and Chemical Engineering, Northwest Normal University,
Lanzhou 730070, China
e-mail: wrf38745779@126.com
e-mail: leizq@nwnu.edu.cn

Vulcan® XC72R (200 mg) was added to the mixture under stirring conditions. The pH of the system was adjusted to ~10 by the dropwise addition of a 5 wt.% KOH/EG solution with vigorous stirring. The mixture was then placed into a flask, and the temperature was maintained at 180°C for 20 h, the resultant was collected by filtration, washed with deionized water five times, and dried in air at 60°C for 12 h.

Afterwards, appropriate amounts of H_2PtCl_6 aqueous solutions were added to another flask. The obtained Ni/C powders were submitted to the flask, and the mixture was stirred for 8 h (Pt/Ni=1:6 in atomic ratio) at 95°C. Subsequently, the resulting powders were collected by filtration and then washed with deionized water until no chloride anion in the filtrate, followed by drying in air at 60°C for 12 h. The Pt-Ni/C catalyst was obtained. For a comparison, the commercially available Pt/C (20 wt.%) and PtRu/C (30 wt.%) were obtained from Johnson Matthey for electrochemical characterizations.

The catalysts were characterized by recording their X-ray diffractometry (XRD) patterns on a Shimadzu XD-3A (Japan), using filtered Cu-Kα radiation. All X-ray diffraction patterns were analyzed using Jade 7.5 of Material Data, Inc.: peak profiles of individual reflections were obtained by a nonlinear least-square fit of the Cu Kα corrected data. Transmission electron microscopy (TEM) was carried out on a Tecnai G220 S-TWIN (FEI Company); the acceleration voltage was 200 kV. The average chemical compositions of Pt-Ni/C catalyst were determined using an IRIS advantage inductively coupled plasma atomic emission spectroscopy (ICP-AES) system (Thermo, America).

The electrochemical measurements of catalysts were performed using an electrochemical work station (CHI604). A common three-electrode electrochemical cell was used for the measurements. The counter and reference electrode were a platinum wire and an Ag/AgCl (3 M KCl) electrode, respectively. The working electrode was a glassy carbon disk (5 mm in diameter). The thin-film electrode was prepared as follows: 5 mg of catalyst was dispersed ultrasonically in 1 mL nafion/ethanol (0.25% Nafion) for 15 min. Eight microliters of the dispersion was transferred onto the glassy carbon disk using a pipette and then dried in the air.

Results and discussion

The carbon-supported Pt-Ni/C samples were synthesized using a sequential reduction process. The carbon-supported Ni nanoparticles were first synthesized by a modified organic colloid method in an ethylene glycol solution. After the synthesis of the Ni nanoparticles supported on Vulcan carbon, the second step involved galvanic displacement of Ni by Pt^{4+} according to the reaction:

$$2Ni + [PtCl_6]^{2-} \rightarrow Pt + 2Ni^{2+} + 6Cl^- \quad (1)$$

The difference between the E^0 values of $Pt/[PtCl_6]^{2-}$ (0.742 V vs NHE) and Ni/Ni^{2+} (0.250 V vs NHE) is adequate for the displacement reaction to be both thermodynamically as well as kinetically favorable. It is generally accepted that minimization of surface energy is one of the main driving forces for encapsulation. Interactions between metals and defective carbon are weaker than that between metals and metals. The practical composition of the Pt-Ni/C catalyst was evaluated by ICP-AES analysis. The particle composition of the prepared catalyst is Pt/Ni=1:3.3 (atomic ratio).

Figure 1 shows the XRD patterns of Pt-Ni/C, Pt/C, and Ni/C catalysts. For comparison, carbon-supported PtNi alloy (PtNi/C, Pt/Ni=3:1 in atomic ratio) catalyst prepared by the polyol method is also shown in this figure. For clarity, the diffraction patterns between 35° and 45° have been enlarged in the inset of Fig. 1. The four peaks of Pt-Ni/C, PtNi/C, and Pt/C catalysts are characteristic of face-centered cubic (fcc) crystalline Pt (alloy), corresponding to the planes (111), (200), (220), and (311), at 2θ values of ca. 40°, 47°, 68°, and 83°, respectively. The (111) peaks of Pt and Ni of the as-deposited electrode without any heat treatment are located at 39.7°and 44.5°, respectively, having the original peak positions of their metallic states.

The diffractograms of Ni/C are indicative of a crystalline structure mainly with amorphous state, which could stem from surface layers (The presence of the first peak is due to the supporting material and the broader second peak indicates the amorphous state of the Ni). Compared with

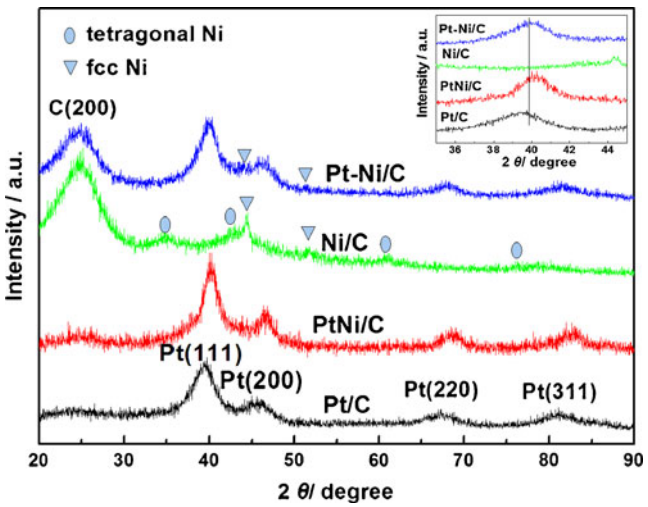

Fig. 1 XRD patterns of Pt/C, PtNi/C, Ni/C, and Pt-Ni/C catalysts. *Inset* The enlarged XRD patterns of Pt/C, PtNi/C, Ni/C, and Pt-Ni/C catalysts

its crystallized counterpart, a metal in an amorphous state holds many more lattice defects and thus could give birth to distinct effects in mediating the electronic structure and/or tuning the atomic arrangement and coordination of the outer shell [17, 18]. Based on this concept, Pt decorating of amorphous Ni core could be expected to decrease the usage of Pt and enhance its catalytic activity at the same time.

However, an important point to be noted here is the simultaneous existence some of Ni in both tetragonal and fcc phases. For fcc Ni, the peaks at 2θ=44.5° and 51.8° correspond to reflections from (111) and (200) planes, respectively; whereas for tetragonal Ni, the same peaks appear because of reflections from (211) and (003) planes. A peak in Ni/C occurs at interplanar spacings of 0.2667 nm assuming a tetragonal crystal structure with space group 14/mcm [19]. It has been reported that a tetragonal Ni-Ob lattice is derived from the fcc Ni lattice by the incorporation of O atoms at the interstitial positions of the latter [20]. The presence of these oxygen atoms, which have larger atomic radii (0.140 nm) compared to Ni (0.1246 nm), strains the Ni lattice and makes it tetragonal.

The inset of Fig. 1 shows that Pt (1 1 1) diffraction angles of Pt-Ni/C samples slightly move to higher positions compared with Pt/C, indicating that PtNi alloy exists in the Pt-Ni/C samples. The reason might be that the freshly reduced Pt atoms on the Ni seeds surface are very active, leading to the easy formation of PtNi alloy and occurrence of the Pt (1 1 1) diffraction peak shift in the XRD patterns [14]. On the other hand, the (1 1 1) diffraction of Pt-Ni/C shifts slightly negative relative to that of PtNi/C, suggesting that Pt-Ni/C catalyst with a low degree of alloy. The mean crystallize size of the particles can be calculated using Debye–Scherrer formula [21], the mean crystallize size of Pt/C, Ni/C, and Pt-Ni/C catalysts is ca. 3.5, 2.5, and 3.3 nm, respectively.

Figure 2a shows TEM image of Pt-Ni/C catalyst and the inset of Fig. 2a shows TEM image of Ni/C nanoparticles. It is noted that the Ni and Pt-Ni nanoparticles are highly dispersed on the carbon support with narrow size distribution. The uniform nanoparticles dispersion of Pt-Ni/C catalyst may result from the precursor Ni nanoparticles distribution on carbon black in the process of the first step Ni/C preparation. The average particle size of Pt-Ni/C catalyst is approximately 3–4 nm obtained by counting one hundred particles. A high resolution transmission electron microscopy study of a series of single Pt-Ni nanoparticles shows that each nanoparticle has a polycrystalline structure (Fig. 2b). The measured distance between the two nearest atom rows for Pt-Ni/C is 0.228 nm, i.e., which is close to the (111) interplanar distance of pure Pt (0.2308 nm),

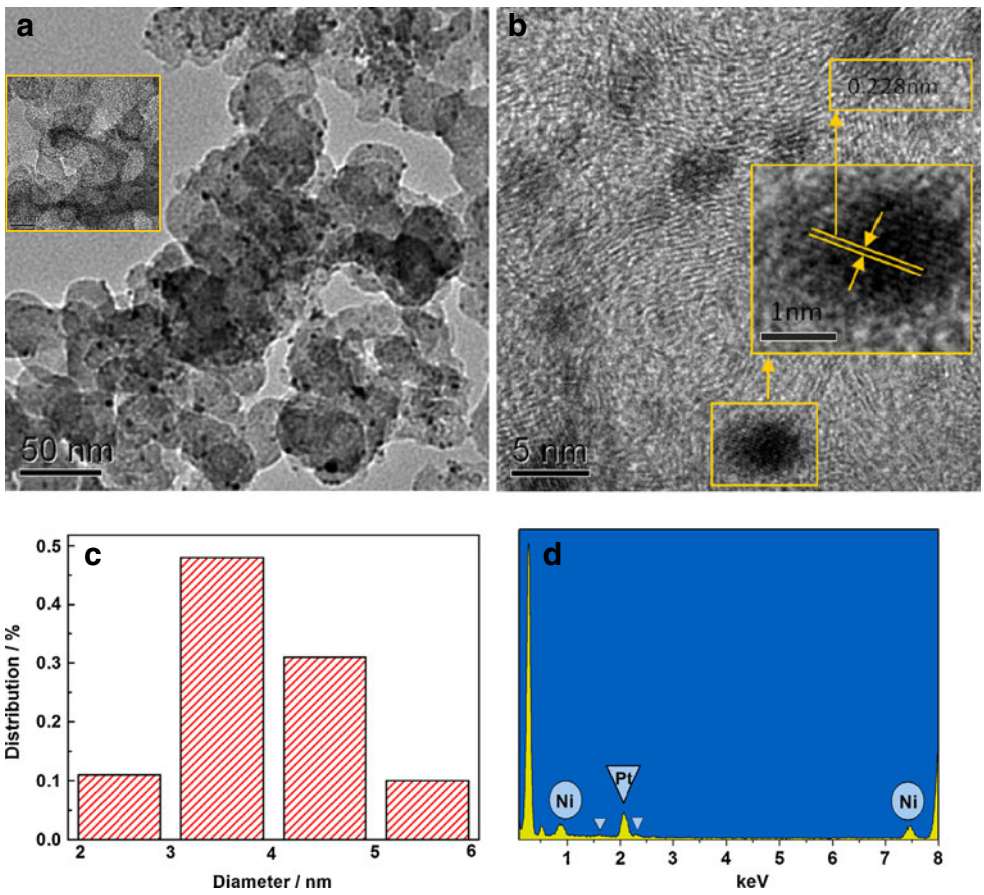

Fig. 2 The **a** TEM and **b** HRTEM images of Pt-Ni/C catalyst. **c** The histograms of particle size distributions of Pt-Ni/C. **d** EDX spectrum of the Pt-Ni/C. *Inset* of **a** TEM image of Ni/C nanoparticle

suggesting Pt atoms are dispersed on the outer layer of Ni particles and not alloyed with Ni nanoparticles. The corresponding particle size distribution histogram (Fig. 2c) of Pt-Ni shows a lognormal distribution accompanied by a relatively narrow size distribution. Most of the metal particles are in the range of 2–6 nm in diameters, and the average particle size is about 3.3 nm. The EDS result of Pt-Ni/C atomic ration of Pt/Ni is 1:3.2 (as shown in Fig. 2d). The Pt/Ni ratios measured by EDS and ICP are in good agreement.

Another evidence for the Pt decorating Ni comes from cyclic voltammetry (CV) as it can be regarded as a surface sensitive technique that only detects the electrochemical properties of surface atoms rather than bulk atoms. Figure 3 shows the CV of Pt/C, PtRu/C and Pt-Ni/C catalysts. For comparison, the CV plot of Ni/C prepared is also shown in the inset of this figure. There is one oxidation peak centered at about 0.3 V on the first forward scan curve and it disappears after four cycles. The voltammogram of Pt-Ni/C resembles that of polycrystalline Pt (hydrogen adsorption/desorption peaks, oxide formation/stripping wave/peak, and a flat double layer region in between), indicating that Pt atoms are separate species on the surface of Ni particles. The electrochemical surface areas (ECSAs) calculated from the hydrogen adsorption/desorption region are 74.43 $m^2\ g^{-1}$ metals for Pt/C, 72.66 $m^2\ g^{-1}$ metals for PtRu/C, and 46.77 $m^2\ g^{-1}$ metals for Pt-Ni/C, respectively. Based on the Pt mass, the ECSAs of Pt-Ni/C are 186.98 $m^2\ g^{-1}$ Pt, which is 2.51 times larger than that of Pt/C catalyst and 3.85 times larger than that of PtRu/C catalyst. The high ECSAs are favorable to electrochemical reaction toward methanol oxidation. The results suggest a simple route of enhancing the catalytic efficiency of Pt-based catalysts is to modify the morphology.

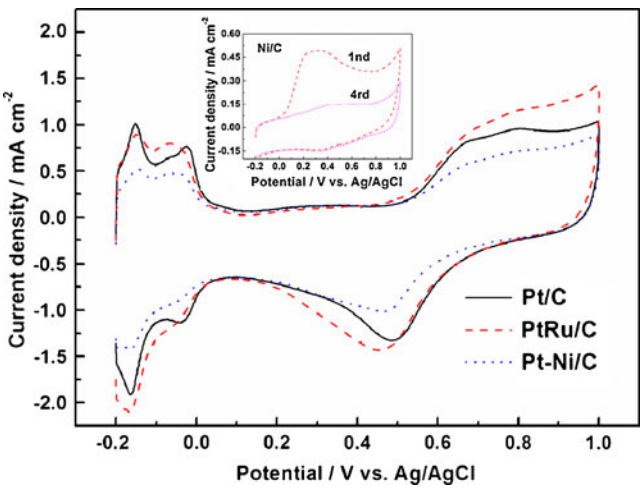

Fig. 3 Cyclic voltammograms of Pt/C, PtRu/C, and Pt-Ni/C catalysts in **a** 0.5 mol L^{-1} H_2SO_4 solution under N_2 atmosphere; scan rate= 50 mV s^{-1}. *Inset* Cyclic voltammograms for Ni/C electrode of the first and fourth cycles, respectively

Activities of the Pt-Ni/C, Pt/C, and PtRu/C catalysts toward anodic oxidation shown in Fig. 4 were also tested in methanol solution with sulfuric acid electrolyte using CV. From Fig. 4, it can be seen that the value of the onset potential for methanol oxidation on Pt-Ni/C, PtRu/C, and Pt/C is Pt/C > PtRu/C > Pt-Ni/C. The lower onset potential indicates a clear evidence for superior electrocatalytic activity for methanol electro-oxidation. Therefore, the Pt-Ni/C catalyst shows relatively good electrocatalytic activity. The mass activity of Pt-Ni/C catalyst at the potential of current maximum is 0.312 A mg_{Pt}^{-1}, which is about 1.56 and 1.24 times as large as those of Pt/C and PtRu/C catalysts, respectively. However, this result does not correspond to the kinetic region but the diffusion-limited region. The mass activities of Pt-Ni/C, PtRu/C, and Pt/C catalysts at the kinetic region (about 0.3 V vs Ag/AgCl) are 0.069, 0.032, and 0.026 A mg_{Pt}^{-1}, respectively. When translate mass activity into specific activity, they are 0.371, 0.458, and 0.350 mA cm^{-2} for Pt-Ni/C, PtRu/C, and Pt/C, respectively. The lower onset potential and higher mass activity of methanol oxidation for the Pt-Ni/C catalyst indicate that it is superior to the commercial Pt/C and PtRu/C catalysts.

The ratio of the forward anodic peak current (I_f) to the reverse anodic peak current (I_b) can be used to describe the tolerance of catalyst to accumulation of carbonaceous species [22]. A higher ratio indicates more effective removal of the poisoning species on the catalyst surface. The I_f/I_b ratio of Pt-Ni/C is 2.47, which is higher than those of Pt/C (1.28) and PtRu/C (1.73), showing better catalyst tolerance of Pt-Ni/C composites.

Tafel plots of the methanol oxidation on the Pt-Ni/C, Pt/C, and PtRu/C catalysts derived from the linear sweep voltammograms in 0.5 M H_2SO_4 solution plus 0.5 M

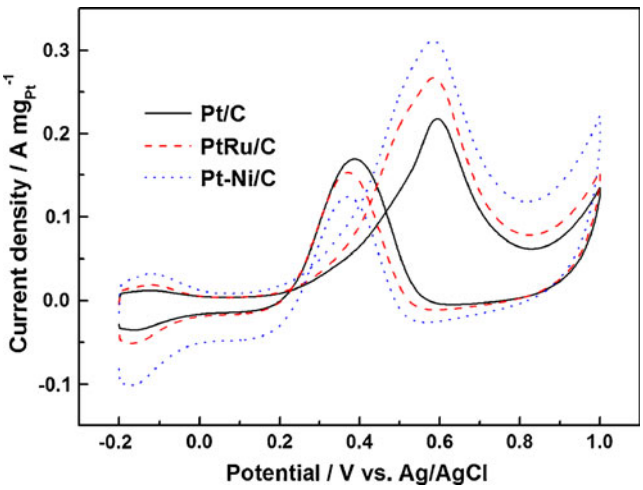

Fig. 4 Cyclic voltammograms of Pt/C, PtRu/C, and Pt-Ni/C catalysts in 0.5 mol L^{-1} CH_3OH + 0.5 mol L^{-1} H_2SO_4 solution under N_2 atmosphere; scan rate=50 mV s^{-1}

CH_3OH at a scanning rate of 5 mV s^{-1} (close to a steady-state polarization curve, not shown here) are shown in Fig. 5. Each plot can be fitted and divided into two linear regions according to the change of Tafel slopes. The first fitted Tafel slopes come within the scope of 47.8 to 79 mV dec^{-1} at low overpotentials, while the second slopes are in the range of 173.4 to 250.0 mV dec^{-1} at high overpotentials. The different of the Tafel slopes values at low and high overpotentials may indicate a possible change of reaction mechanism or at least a transformation of rate-determining step at different potential range [23]. From the aspect of kinetic theory, the Tafel slope at low potentials for methanol oxidation indicates that the unit reaction involving the splitting of the first C–H bond of methanol molecules with the first electron transfer is the rate-determining step at low overpotential [24]. The change of the Tafel slopes at high potentials may be attributed to the insufficient compensation of methanol oxidation for the rapid oxidation reaction on the electrode surface, and mass transfer of methanol at high overpotential is hypothesized to be the rate-determining step [25].

Chronoamperometric experiment shown in Fig. 6 was carried out to observe the stability and possible poisoning of the catalysts under short time continuous operation. For each catalyst, the decay in the methanol oxidation is different. It is clear that the current at the Pt-Ni/C and PtRu/C catalysts electrodes at 1,200 s is 0.0122 and 0.0049 A mg_{Pt}^{-1}, respectively. The Pt-Ni/C composite electrode shows more stability than the PtRu/C electrode when the electrodes are compared under identical experimental conditions.

The electrocatalytic cycling stabilities of the Pt-Ni/C and PtRu/C in 0.5 M CH_3OH + 0.5 M H_2SO_4 solution have also been compared using CV cycling, as shown in Fig. 7.

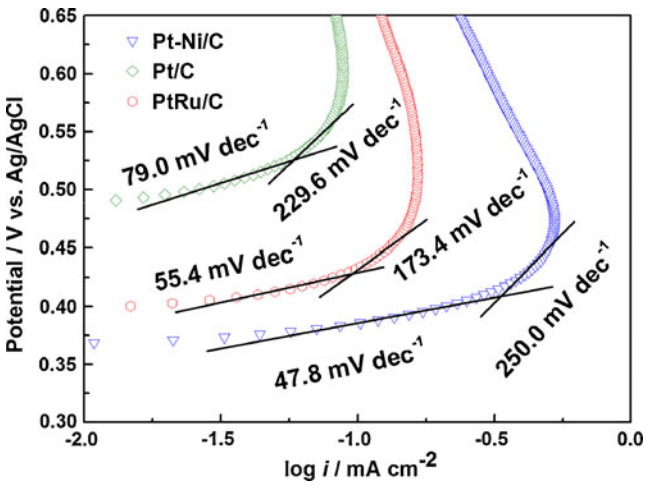

Fig. 5 Tafel plots of methanol oxidation on Pt/C, PtRu/C, and Pt-Ni/C catalysts in 0.5 mol L^{-1} CH_3OH + 0.5 mol L^{-1} H_2SO_4 solution under N_2 atmosphere. Scan rate=5 mV s^{-1}

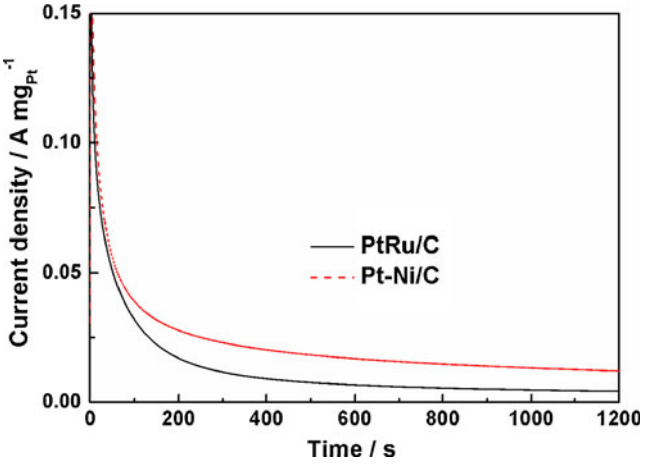

Fig. 6 Chronoamperometry curves of PtRu/C and Pt-Ni/C for methanol oxidation, polarized at a constant potential of 0.6 V vs Ag/AgCl at room temperature

After 100 CV cycling, the mass activity of Pt-Ni/C catalyst is about 1.28 times as large as that of PtRu/C catalyst. It can be seen that the loss of the electrocatalytic activity for Pt-Ni/C is lower than that of PtRu/C catalyst, further indicating that the present Pt-Ni/C has good stability.

The activity of metal alloy catalysts for anodic reaction is generally characterized by a prominent bifunctional effect [26]. A secondary metal catalyst in a bifunctional mechanism is able to assist Pt to oxidatively remove poisoning species from the surface. This is because the secondary metal catalyst is capable of generating active oxygen species, OH_{ads}, through dissociative absorption of water. Compared to the Pt/C and PtRu/C, the excellent catalytic activity of the Pt-Ni/C is considered that: (a) the higher exposure and utilization of Pt can be achieved when most of Pt atoms are separated on the surface without alloyed with Ni [14]. Pt-Ni/C catalyst has a larger surface area,

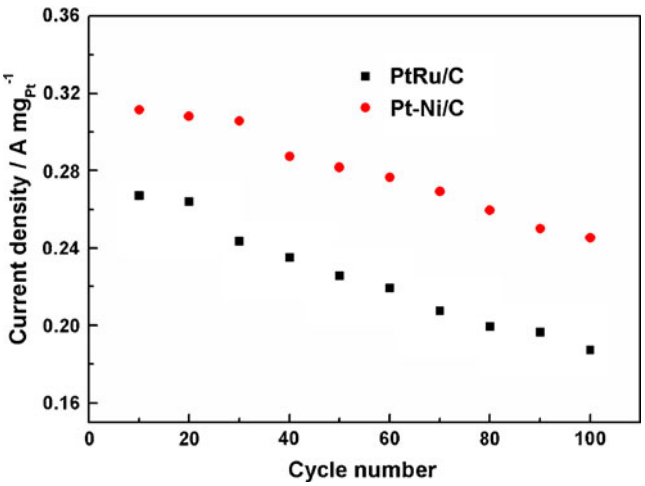

Fig. 7 Electrocatalytic cycling stability of Pt-Ni/C and PtRu/C

which provides more active sites and results in high electrocatalytic activity. (b) Pt catalytic activity for methanol oxidation can be improved as the Ni nanoparticles change the electronic structure of Pt [9]. The bifunctional effect between Ni and Pt is more effectively than Pt. (c) The presence of Ni oxides in the catalyst provides an oxygen source for CO oxidation and then promoted methanol oxidation.

Conclusions

In this article, a modified solution-phase reduction method was used to prepare a Pt-Ni/C catalyst, which has a mean particle size of 3.3 nm and uniform nanoparticles dispersion on carbon support. Although the specific activity of the Pt-Ni/C similar with that of Pt/C and lower with that of PtRu/C, the mass activity at the kinetic region of Pt-Ni/C catalyst is about 2.65 times and 2.15 as large as that of Pt/C and PtRu/C catalysts, respectively. After 100 CV cycling, the loss of the electrocatalytic activity for Pt-Ni/C is lower than that of PtRu/C catalyst. The Pt-Ni/C catalyst not only exhibits better catalytic activity and resistance to carbonaceous intermediate poison but also decreases wastage of expensive Pt. These encouraging findings could be expanded to other catalysts and could open up a new direction in catalysis.

Acknowledgments We would like to thank the State Natural Science Foundation of China (Project No. 20774074), the Key Project of Ministry of Education Foundation of China (Project No. 209129), and the scientific and technical innovation project of northwest normal university (nwnu-kjcxgc-03-63) for financially supporting this work.

References

1. Huang SY, Chang CM, Wang KW, Yeh CT (2007) Chemphyschem 8:1774–1777
2. Yang H, Coutanceau C, Léger JM, Alonso-Vante N, Lamy C (2005) J Electroanal Chem 576:305–313
3. Yang H, Vogel W, Lamy C, Alonso-Vante N (2004) J Phys Chem B 108:11024–11034
4. Colón-Mercado HR, Kim H, Popov BN (2004) Electrochem Commun 6:795–799
5. Yang HZ, Zhang J, Kumar S, Zhang HJ, Yang RD, Fang JY, Zou SZ (2009) Electrochem Commun 11:2278–2281
6. Stamenković V, Schmidt TJ, Ross PN, Markovic NM (2002) J Phys Chem B 106:11970–11979
7. Drillet JF, Ee A, Friedemann J, Kötz R, Schnyderb B, Schmidt VM (2002) Electrochim Acta 47:1983–1988
8. Zhao Y, YF E, Fan LZ, Qiu YF, Yang SH (2007) Electrochim Acta 52:5873–5878
9. Park KW, Choi JH, Kwon BK, Lee SA, Sung YE (2002) J Phys Chem B 106:1869–1877
10. Park KW, Choi JH, Sung YE (2003) J Phys Chem B 107:5851–5856
11. Liu F, Lee JY, Zhou WJ (2004) J Phys Chem B 108:17959–17963
12. Antolini E, Salgado JRC, Gonzalez ER (2006) Appl Catal B: Environ 63:137–149
13. Lee KS, Park IS, Park HY, Jeon TY, Cho YH, Sung YE (2009) J Electrochem Soc 156:B1150–B1155
14. Fu XZ, Liang Y, Chen SP, Lin JD, Liao DW (2009) Catal Commun 10:1893–1897
15. Wang RF, Zhang Z, Wang H, Lei ZQ (2009) Electrochem Commun 11:1089–1091
16. Wang RF, Li H, Feng HQ, Wang H, Lei ZQ (2010) J Power Sources 195:1099–1102
17. Zhang XB, Yan JM, Han S, Shioyama H, Xu Q (2009) J Am Chem Soc 131:2778–2279
18. Yan JM, Zhang XB, Han S, Shioyama H, Xu Q (2008) Angew Chem Int Ed 47:2287–2289
19. Roy A, Srinivas V, Ram S, De Toro JA (2005) Phys Rev B 71:184443-1-10
20. Roy A, Srinivas V, Ram S, De Toro JA, Riveiro JM (2004) J Appl Phys 96:6782–6788
21. Wang RF, Wang H, Wei BX, Wang W, Lei ZQ (2010) Int J Hydrogen Energy 35:10081–10086
22. Guo SJ, Dong SJ, Wang E (2010) ACS Nano 4:547–555
23. Zhu J, Cheng F, Tao Z, Chen J (2008) J Phys Chem C 112:6337–6345
24. Wu G, Li L, Xu BQ (2004) Electrochim Acta 50:1–10
25. Kim YJ, Hong WH, Woo SI, Lee HK (2006) J Power Sources 159:491–500
26. Batista EA, Malpass GRP, Motheo AJ, Iwashita T (2004) J Electroanal Chem 571:273–282